RSC Advances

PAPER

View Article Online
View Journal | View Issue

Cite this: *RSC Adv.*, 2020, **10**, 28383

Size-dependent magnetic and magnetothermal properties of gadolinium silicide nanoparticles

Muhammad Nauman, *[ab] Muhammad Hisham Alnasir,[b] Muhammad Asif Hamayun,[b] YiXu Wang,[cd] Michael Shatruk [c] and Sadia Manzoor*[b]

Received 19th June 2020
Accepted 17th July 2020

DOI: 10.1039/d0ra05394e

rsc.li/rsc-advances

Gadolinium silicide (Gd_5Si_4) nanoparticles are an interesting class of materials due to their high magnetization, low Curie temperature, low toxicity in biological environments and their multifunctional properties. We report the magnetic and magnetothermal properties of gadolinium silicide (Gd_5Si_4) nanoparticles prepared by surfactant-assisted ball milling of arc melted bulk ingots of the compound. Using different milling times and speeds, a wide range of crystallite sizes (13–43 nm) could be produced and a reduction in Curie temperature (T_C) from 340 K to 317 K was achieved, making these nanoparticles suitable for self-controlled magnetic hyperthermia applications. The magnetothermal effect was measured in applied AC magnetic fields of amplitude 164–239 Oe and frequencies 163–519 kHz. All particles showed magnetic heating with a strong dependence of the specific absorption rate (SAR) on the average crystallite size. The highest SAR of 3.7 W g^{-1} was measured for 43 nm sized nanoparticles of Gd_5Si_4. The high SAR and low T_C, (within the therapeutic range for magnetothermal therapy) makes the Gd_5Si_4 behave like self-regulating heat switches that would be suitable for self-controlled magnetic hyperthermia applications after biocompatibility and cytotoxicity tests.

1. Introduction

Magnetically induced hyperthermia is proposed as an alternative anticancer therapy in which the heat produced by magnetic nanoparticles (MNPs) in radio frequency (RF) magnetic fields is used to destroy cancerous cells or retard their growth.[1–11] The therapeutic action is due to the magnetothermal effect by which MNPs transform alternate current (AC) magnetic field energy into heat by different magnetic loss mechanisms, such as Néel and Brownian losses.[3] The heating efficiency of the MNPs is quantified in terms of the specific absorption rate (SAR), which is the amount of heat dissipated per unit time per unit mass of particles. The SAR depends on external factors, such as the frequency and amplitude of the applied AC field,[12,13] as well as on structural and magnetic properties of the MNPs, such as magnetization, coercivity, magnetic anisotropy (including surface anisotropy), *etc.*, which in turn are strongly dependent on the average crystallite size. Producing MNPs with high SAR values is important for magnetothermal therapy in order to reduce the dosage of the hyperthermia agent.[14]

Magnetic hyperthermia and thermo-ablation are the two main treatment techniques that can be employed for destroying cancer cells through heat. Both are localized modes of treatment that have fewer side effects than conventional chemo- and radiotherapies. Thermoablation involves high temperature treatment (T ~55 °C or 328 K) for a short period of time, typically 10 min. This is favorable on account of time saving but has harmful side effects like shock syndrome and inflammatory response which can happen due to accretion of necrotic material. Hyperthermia involves heating up to the therapeutic temperatures of 42–47 °C (315–320 K) for a few hours. Because of the extended treatment time, the final temperature attained is difficult to control and can exceed the therapeutic limit leading to overheating and spot-burning, causing damage to healthy tissue as well. Therefore, a much-preferred modality of magnetothermal therapy is self-controlled magnetic hyperthermia, in which the Curie temperature (T_C) of the magnetic nanomaterial is tuned to lie in the therapeutic range, between 315 and 320 K.[15] Upon achieving these temperatures, the heating capability of such materials reduces drastically due to the transition to the paramagnetic state at T_C. This prevents overheating, burning and possible necrosis of healthy tissue.

To get a high hyperthermia response from small dosages of the hyperthermia agent, MNPs with high magnetic response should be used, but these also usually have very high Curie temperatures. Most compounds proposed as potential candidates for magnetic hyperthermia have T_C values that lie well above the therapeutic range, even for very small sized MNPs. For

[a]*Department of Physics, Kyungpook National University, Daegu 41566, Korea. E-mail: nouman.kakakhail@gmail.com*

[b]*Department of Physics, COMSATS University Islamabad, 45550, Pakistan. E-mail: sadia_manzoor@comsats.edu.pk*

[c]*Department of Chemistry and Biochemistry, Florida State University, Tallahassee, FL 32306, USA*

[d]*School of Materials Science and Engineering, University of Science and Technology Beijing, Beijing, 100083, P. R. China*

example, magnetite (Fe_3O_4) has $T_C = 738$ K for 6.4 nm diameter particles,[16] while for 10 nm maghemite (γ-Fe_2O_3) nanoparticles $T_C = 546$ K has been reported.[17] Such high T_C values make these materials unsuitable for self-controlled hyperthermia applications. Several attempts have been made to tune the T_C of ferrites and rare earth manganites and bring it within the therapeutic range, but this results in loss of magnetization and lower SAR's. Such a problem can be resolved by using a system that retains its magnetization at the nanoscale without any significant loss in the SAR and magnetothermal response. Bulk gadolinium silicide (Gd_5Si_4) has the distinct advantage that it has high bulk magnetization 100 emu g^{-1} and a low $T_C = 340$ K,[18] which can be further reduced by ball milling or doping and brought within the therapeutic range for self-controlled hyperthermia applications. This unique combination of high magnetization and low T_C endows this material with multifunctional properties. For example El-Gendy *et al.* have shown that Gd_5Si_4 act equivalent to commercially available superparamagnetic iron oxide nanoparticles (SPIONs) for enhancing T2 contrast in magnetic resonance imaging (MRI).[19] The high magnetization of Gd_5Si_4 ensures that the material can be used in small dosages, making it cost-effective. Thus, they can be used as "theranostic" agents[20] due to their simultaneous diagnostic (*e.g.* in MRI) and therapeutic properties as agents of self-controlled magnetic hyperthermia as has been shown in our work.

Despite these attractive properties there is relatively little work on biomedical applications of Gd_5Si_4 nanoparticles.[21] The synthesis of Gd_5Si_4 MNPs *via* wet chemistry is a challenging task because gadolinium oxidizes very readily resulting in stark reduction in magnetization. Producing Gd_5Si_4 by ball-milling in presence of suitable surfactants avoids the oxidation of gadolinium and also provides a high yield and well-controlled scalability of the nanoparticles.

In this work, we have synthesized bulk Gd_5Si_4 by arc melting and reduced it to the nanoscale through surfactant-assisted ball milling. The influence of milling time and milling speed on structural, magnetic and magnetothermal properties of MNPs has been investigated to assess their efficacy as agents of self-controlled magnetic hyperthermia. We have successfully reduced the Curie temperature of Gd_5Si_4 nanoparticles to within the therapeutic range. This reduction in the particle size and T_C afforded a maximum SAR values of 3.7 W g^{-1} for Gd_5Si_4 nanoparticles milled at 200 rpm for 10 min.

2. Experimental procedure

Synthesis

Bulk Gd_5Si_4 samples were prepared by arc melting stoichiometric mixtures of Gd (purity 99.99 wt%) and Si (99.99 wt%). The powders of elements were pressed into pellets and arc-melted. All operations were performed in an argon-filled glovebox (O_2 content < 1 ppm). Each as-cast specimen was flipped over and re-melted 2–3 times in order to obtain a homogeneous ingot. The ingots were placed in carbonized silica tubes (10 mm inner diameter), which were sealed under vacuum ($<10^{-2}$ mbar) and transferred into a Lindberg Blue M furnace (Thermo Electron Corporation). All samples were annealed at 1100 °C for 24–48 h and cooled down to room temperature by turning off the furnace. Weight loss after arc-melting was less than 1%.

Ball milling

The arc-melted bulk ingots were first ground with a mortar and a pestle in methanol for 1 h and then transferred to a planetary micro-mill (FRITSCH PULVERISETTE Premium Line 7) with 2 mm diameter zirconia balls, using a ball to sample mass ratio of 5 : 1. Milling was done in inert argon atmosphere. The amount of surfactant (oleic acid) used was 10% of the sample mass. *n*-Hexane of 99.8% purity was used as a solvent. Two series of Gd_5Si_4 samples were milled at 200 rpm and 500 rpm for 10, 30, 50, 80, and 100 min. All samples were labeled according to the milling speed and milling time; for example, the label BM-200-100 indicates the sample milled at 200 rpm for 100 min.

Physical measurements

The structure of the bulk and milled materials was examined using powder X-ray diffraction (PXRD) on a Panalytical XPert Pro diffractometer with Cu-Kα radiation ($\lambda = 1.54187$ Å). A transmission electron microscope (JEOL JEM-ARM200cF) was used to investigate the morphology of the samples and obtain selected area electron diffraction (SAED) patterns. Chemical analysis of selected samples was done using energy dispersive electron spectroscopy. Field and temperature dependent magnetization measurements were performed using a Quantum Design Versa Lab magnetometer. Time-dependent calorimetric measurements, to determine the SAR values, were made using a nanoTherics Magnetherm® unit. The capacitors and RF coil combinations in this system allow the amplitude and frequency of the magnetic field to be varied in the ranges of 163–238 kHz and 164–239 Oe, respectively. A Nomad™ fiber-optic thermometer was used to log the temperature of the sample that was placed in a thermally insulated vial before being exposed to the magnetic field.

3. Results and discussion

Fig. 1a and b show the PXRD patterns of Gd_5Si_4 nanoparticles prepared by surfactant-assistant ball milling at 200 and 500 rpm for 10, 30, 50, 80, and 100 min. All PXRD patterns contain dominant peaks of the ferromagnetic Gd_5Si_4 phase (ICSD-01-087-2319) and small impurity peaks of GdSi (ICSD-01-072-0705) and Gd_5Si_3 (ICSD-00-024-1288), which are known to be very difficult to remove even after high temperature treatment.[18,22] Since GdSi is antiferromagnetic and Gd_5Si_3 is paramagnetic at room temperature, their presence in small quantities is not expected to affect the magnetic properties of our samples in any significant manner. The lattice parameters obtained for BM-200-10 and BM-500-10 are $a = 7.4714$ Å, $b = 14.7111$ Å and $c = 7.7359$ Å and $a = 7.4691$ Å, $b = 14.7114$ Å and $c = 7.7311$ Å, respectively. They correspond well to the reported Gd_5Si_4 structure with $a = 7.4738$ Å, $b = 14.7240$ Å and $c = 7.7362$ Å (ICSD-01-087-2319). Increasing the milling time to 100 min changed the lattice parameters by <0.1%.

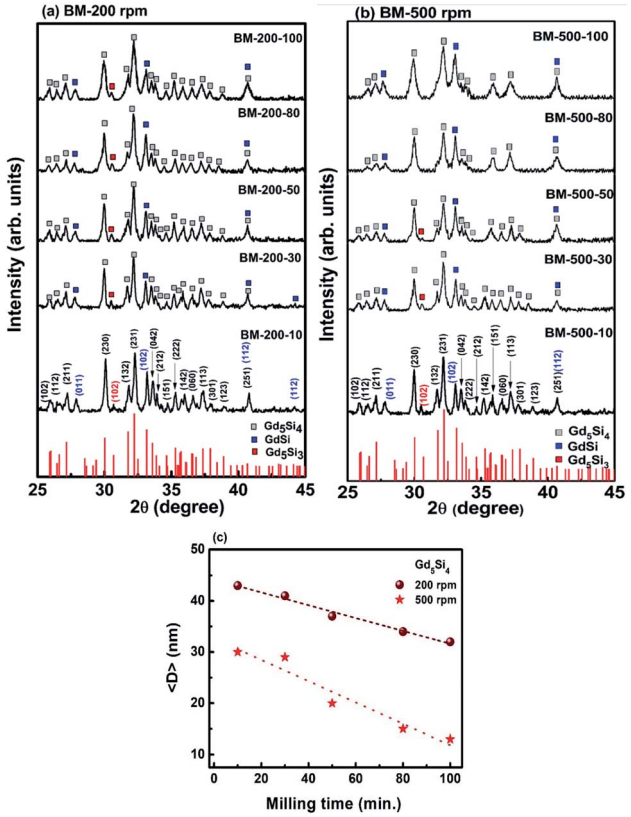

Fig. 1 PXRD patterns of Gd_5Si_4 samples ball milled in oleic acid at (a) 200 rpm and (b) 500 rpm for 10, 30, 50, 80, and 100 min. The lowermost panels in (a) and (b) show the reference pattern of Gd_5Si_4 (ICSD 01-087-2319) for comparison. (c) The average crystallite size $\langle D \rangle$ of Gd_5Si_4 nanoparticles obtained by milling at 200 rpm and 500 rpm as a function of milling time. The straight lines are meant as guide to the eye.

The increase in the milling speed results in partial loss of crystallinity and peak broadening, indicating a reduction in the average crystallite size for samples milled at 500 rpm. The average crystallite sizes $\langle D \rangle$ were estimated from the PXRD data using the Scherer formula. Ball-milling is a high energy process that may lead to some internal stresses that could contribute to the peak broadening. However, since the bulk Gd_5Si_4 samples were very brittle and could be easily crushed in a mortar and pestle, we believe that these effects are small in comparison to size-induced broadening. This is corroborated by the fact that the largest change in the lattice parameters of all milled samples was less than 0.1%. By varying both the milling speed and milling time, we are able to obtain a wide range of crystallite sizes (13–43 nm), which significantly affect the magnetic and magnetothermal properties of our samples, as will be shown below. The decrease in $\langle D \rangle$ with milling time is shown in Fig. 1c for sample milled at 200 and 500 rpm.

Fig. 2 shows representative results of the quantitative EDX elemental analysis of samples BM-200-80 and BM-200-100. Dominant peaks of Gd and Si can be seen, together with a small oxygen admixture, possibly due to minor surface oxidation. Copper and carbon peaks are due to the lacey carbon-coated grid.

Fig. 3a shows a TEM image of sample BM-200-100. There are strongly agglomerated sub-100 nm particles that could not be separated due to their strong dipolar interactions. Fig. 4b and c show the SAED patterns for samples BM-200-100 and BM-500-100, respectively. Progressive loss of crystallinity can be seen in the weakening of the diffraction spots with increasing milling speed.

Magnetization hysteresis loops of the samples were measured at 300 K in applied fields up to ±15 kOe (Fig. 4). All samples show soft ferromagnetic behavior with coercivities lying in the range of 8–29 Oe and 42–87 Oe for the series milled at 200 rpm and 500 rpm, respectively. The magnetization of Gd_5Si_4 nanoparticles does not saturate at 15 kOe, possibly because of some oxidation and surface spin disorder. We observe a significant decrease in magnetization with increasing milling speed and milling time. The low field region displayed in the insets of Fig. 4 shows a magnified view of the coercivity of these samples.

The coercivity H_c and maximum magnetization as functions of milling time and average crystallite size $\langle D \rangle$ for the Gd_5Si_4 samples milled at 200 and 500 rpm are shown in Fig. 5. Since the magnetization does not saturate in these samples, we have plotted the value of the magnetization obtained at 15 kOe (M @ 15 kOe), which is the maximum field used in our measurements. The M @ 15 kOe value decreases with the increase in the milling time and speed

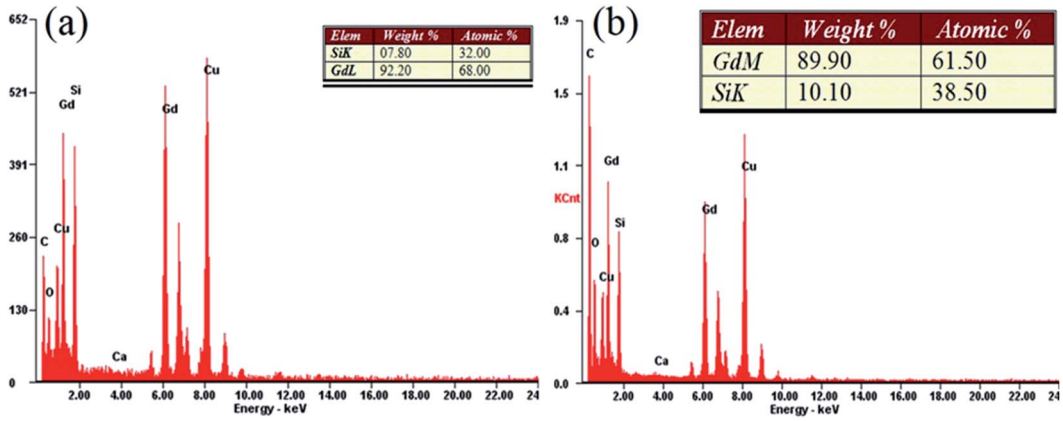

Fig. 2 Energy dispersive X-ray analysis of sample BM-200-80 (a) and BM-200-100 (b).

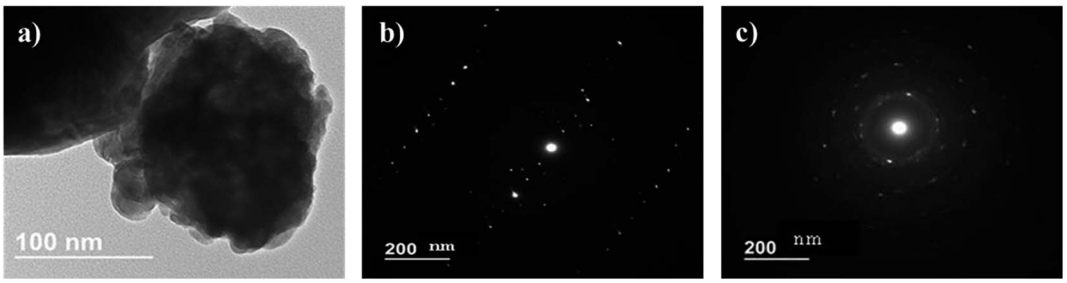

Fig. 3 (a) TEM image of sample BM-200-100. Panels (b) and (c) show the SAED patterns for samples BM-200-100 and BM-500-100.

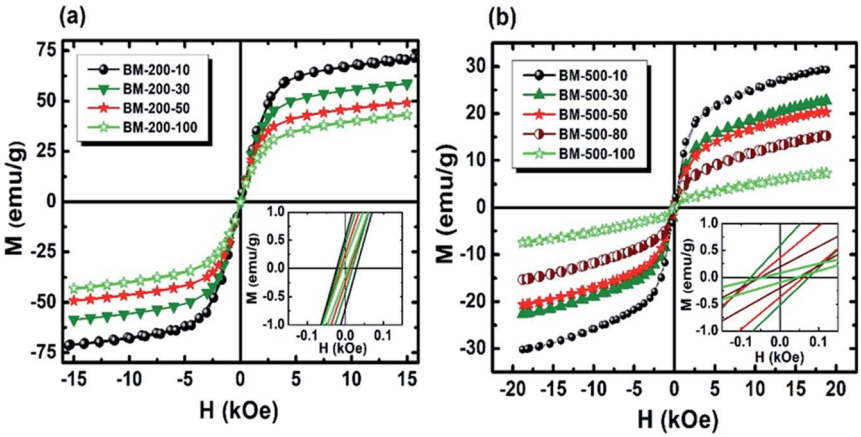

Fig. 4 Room temperature M–H loops of Gd_5Si_4 samples milled for 10, 30, 50, 80, and 100 min at (a) 200 rpm and (b) 500 rpm. The inset shows the coercivity at low field.

(Fig. 5b). This decrease correlates well with the decrease in the average crystallite size (Fig. 5c) established by the PXRD measurements (Fig. 1c). The coercivity increases with higher milling speed and decreases with longer milling times, reaching minimum values of 8 Oe and 42 Oe for samples milled at 200 rpm and 500 rpm, respectively (Fig. 5a). Fig. 5c shows the coercivity and magnetization of all samples as a function of their average crystallite size $\langle D \rangle$. The panel on the left (yellow) shows the data for the series milled at 200 rpm while that on the right shows similar data for samples milled at 500 rpm. The decrease in coercivity H_C with average crystallite size $\langle D \rangle$ indicates that these particles are in the single-domain regime.[23] The magnetization of all samples decreases with increased milling speed, while their coercivity increases. Aggressive milling at 500 rpm produces a more defect-ridden surface layer or shell that is largely amorphous and magnetically dead. The formation of this surface layer reduces the magnetization and at the same time increases the coercivity, as has been observed in core–shell nanoparticles.[24,25] Thus, by varying the milling time and milling speed, we are able to obtain a wide range of crystallite sizes (13–43 nm) with coercivities varying between 8 and 87 Oe and magnetization M @ 15 kOe in the range of 7–73 emu g^{-1}.

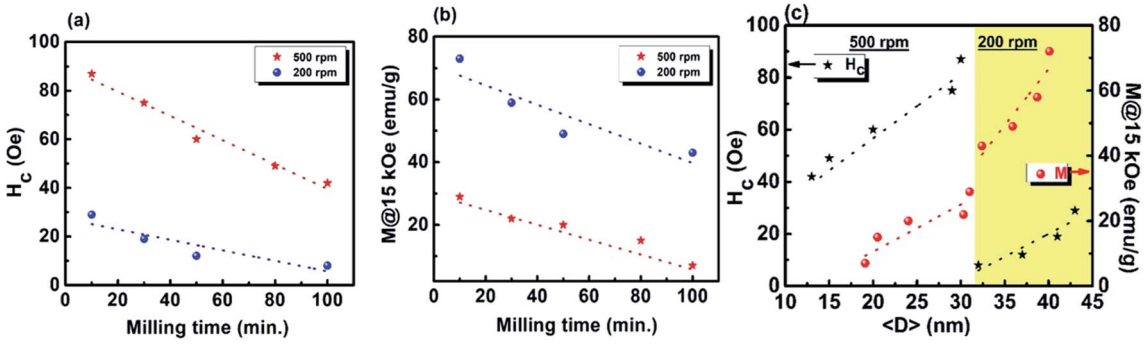

Fig. 5 Dependences of (a) coercivity and (b) maximum magnetization (M @ 15 kOe) on milling time and milling speed, (c) coercivity and magnetization as a function of average crystallite size $\langle D \rangle$ for Gd_5Si_4 samples milled at 200 and 500 rpm. The straight lines are guide to the eye.

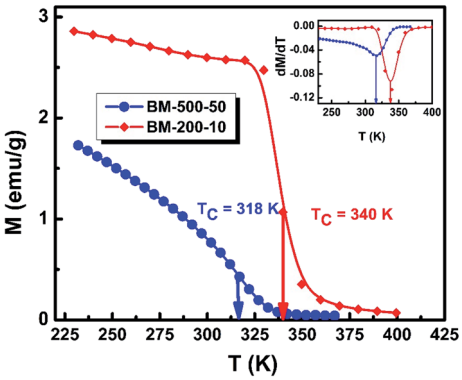

Fig. 6 M–T curves of Gd_5Si_4 samples BM-500-50 and BM200-10 measured in $H = 100$ Oe after cooling in zero field. The inset shows the first derivative $\frac{dM}{dT}$ of the thermal demagnetization curve to obtain T_C for both samples.

To investigate the effect of milling time and milling speed on the Curie temperature (T_C), we measured the thermal demagnetization of BM-200-10 and BM-500-50 samples in the zero-field-cooled (ZFC) mode in a static field of 100 Oe in the temperature range 240–420 K. The results obtained are shown in Fig. 6, where the inset shows the determination of the magnetic phase transition temperature as the minimum of the (dM/dT) curve.[26,27] The BM-200-10 sample shows an abrupt ferromagnetic-like increase in magnetization at ~340 K, which is identical to the T_C of bulk Gd_5Si_4. Increasing milling time and speed for sample BM-500-50 broadens the transition between the paramagnetic and ferromagnetic states while lowering the T_C to 318 K. The magnetic ordering temperature can thus be varied systematically by controlling the size of the Gd_5Si_4 MNPs and brought in the range suitable for self-controlled hyperthermia applications, *i.e.*, between 315 K and 320 K. This is important because it imposes an intrinsic check on the heat dissipation of the MNP's, thereby avoiding the possibility of overheating and spot-burning in magnetothermal therapy.

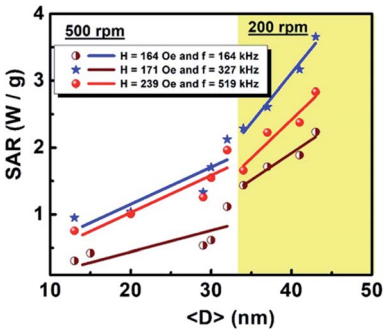

Fig. 8 Dependence of the specific absorption rate (SAR) on the crystallite size $\langle D \rangle$ of Gd_5Si_4 samples milled at 200 and 500 rpm.

The heating potential of Gd_5Si_4 was investigated through magnetothermal measurements carried out on 43 mg of the milled samples in AC magnetic fields of amplitude ranging between 164–239 Oe and frequencies between 163–519 kHz. Fig. 7a and b shows representative heating measurements of samples milled at 200 and 500 rpm, respectively. These measurements were carried out in an AC magnetic field of amplitude $H_{max} = 171$ Oe and frequency $f = 327$ kHz. The insets show the decrease in the final stable temperature T_S (obtained after 85 s exposure to the AC field) with average crystallite size $\langle D \rangle$.

The initial heating rates $\left(\frac{dT}{dt}\right)_{t=0}$ were extracted from the heating curves and used to determine the specific absorption rate (or SAR) according to the equation, $SAR = c\left(\frac{dT}{dt}\right)_{t=0}\frac{m_{sample}}{m_{magn.}}$, where c is the specific heat capacity of the sample, $m_{magn.}$ is the fraction of magnetically active element in the sample, m_{sample} is the mass of the sample, and the derivative $\left(\frac{dT}{dt}\right)_{t=0}$ is the initial slope of the heating curve. For Gd_5Si_4, $c = 0.404$ J g^{-1} K^{-1} (ref. 28) was used. Fig. 8 shows the SAR values obtained from Fig. 7a and b as a function of the average crystallite size for three different combinations of AC

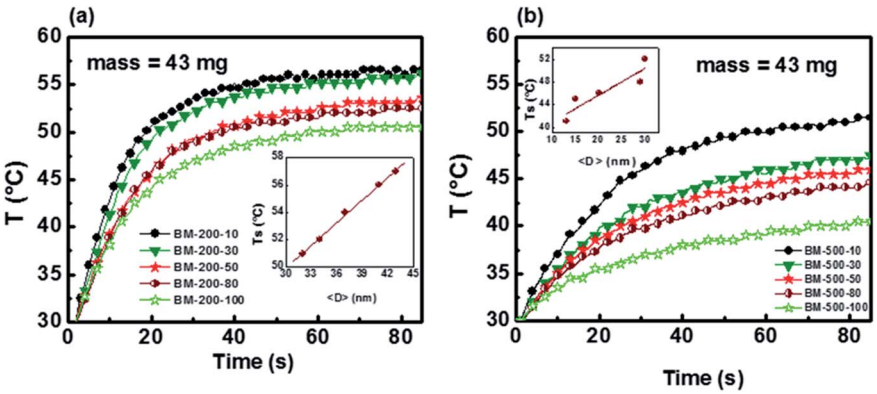

Fig. 7 Heating curves of series (a) BM-200 and (b) BM-500 measured in AC magnetic field of amplitude 171 Oe and frequency 327 kHz. The graphs show the change in temperature for 43 mg of the powder samples. The insets in both graphs show the dependence of final temperature T @ 85 s on average crystallite size $\langle D \rangle$.

Table 1 Comparison of the measured Curie temperature (T_C) and specific absorption rate (SAR), with reported literature

System	T_C (K)	SAR (W g^{-1})
Gd_5Si_4	318 ($\langle D\rangle = 43$ nm)	3.7 ($\langle D\rangle = 43$ nm, $H = 171$ Oe, $f = 327$ kHz)
Fe_3O_4	738 ($\langle D\rangle = 6.4$ nm)[32]	0.5 ($\langle D\rangle = 140$ nm, $H = 1257$ Oe, $f = 820$ kHz)[33]
Fe_2O_3	585 ($\langle D\rangle = 6$ nm)[34]	0.5 ($\langle D\rangle = 9.2$ nm, $H = 133$ Oe, $f = 500$ kHz)[35]
$CoFe_2O_4$	820 ($\langle D\rangle = 40$ nm)[36]	0.04 ($\langle D\rangle = 13.5$ nm, $H = 133$ Oe, $f = 500$ kHz)[35]
$NiFe_2O_4$	860 ($\langle D\rangle = 5.6$ nm)[37]	0.43 ($\langle D\rangle = 9.2$ nm, $H = 133$ Oe, $f = 500$ kHz)[35]
$CuFe_2O_4$	770 ($\langle D\rangle = 22.1$ nm)[37]	0.27 ($\langle D\rangle = 9.4$ nm, $H = 133$ Oe, $f = 500$ kHz)[35]
$ZnFe_2O_4$	800 ($\langle D\rangle = 8$ nm)[38]	0.07 ($\langle D\rangle = 9$ nm, $H = 133$ Oe, $f = 500$ kHz)[35]

field amplitude and frequency. Within the range of sizes investigated, SAR increases linearly with increasing crystallite size $\langle D\rangle$, as is expected for particle sizes in the single domain regime.[29] The value of the SAR for a given $\langle D\rangle$ depends on both the amplitude and frequency of the AC field.[3] The highest SAR value of 3.7 W g^{-1} was obtained for BM-200-10. The Gd_5Si_4 nanoparticles show a higher magnetothermal response at lower fields and frequencies that those of Fe_3O_4 nanoparticles measured at 820 kHz and 1.2 kOe[30] and at 340 kHz and 340 Oe.[31]

Table 1 shows a comparison of the key performance indicators of Gd_5Si_4 and other systems most commonly reported as potential agents of magnetic hyperthermia. The first row represents our experimental results and one can see that the T_C for our samples is significantly lower than that of other systems shown. The T_C of magnetite and maghemite, which are the most commonly proposed materials for biomedical applications, lie well beyond the therapeutic limit even for particles as small as 6 nm. This low T_C of the Gd_5Si_4 nanoparticles means that they stop heating once therapeutic temperatures are achieved, thereby preventing overheating and spot heating of tissue. This is an important result, more so because the SAR or our sample is also higher than that of the ferrites shown in Table 1, some of which have been measured at comparable fields and frequencies.

4. Conclusions

We have investigated the dependence of the magnetic and magnetothermal properties of ball-milled Gd_5Si_4 nanoparticles on their average crystallite size $\langle D\rangle$. By varying the milling time and milling speed, a wide range of crystallite sizes (13–43 nm) could be produced within the single domain regime.

All nanoparticles studied in this work show a linear dependence of the specific absorption rate (SAR) on the average crystallite size. The maximum SAR obtained was 3.7 W g^{-1}. Most significantly, it was found that the reduction in particle size by ball milling can successfully reduce the Curie temperature to lie in the range required for self-controlled magnetic hyperthermia, *i.e.* 315–320 K. This is a distinct advantage of Gd_5Si_4 over other potential candidates for magnetic hyperthermia. Although rare earth based compounds are generally more expensive than some commercially available iron oxide nanoparticles, the high SAR values of these nanoparticles means that they are required in very low dosages to attain the required therapeutic temperaures. Above all, the Gd_5Si_4 nanoparticles investigated in our work can act as self-regulating heat switches because of their low T_C, and this makes them ideal agents for self-controlled magnetic hyperthermia.

Conflicts of interest

There are no conflicts to declare.

Acknowledgements

This work was supported by the Higher Education Commission (Govt. of Pakistan) and USAID under the Pak-US S&T Cooperation Program Phase-V [Grant No. 5-764/PAK-US/HEC/2013/198] and in part by the National Science Foundation (award DMR-1905499 to M. S.). Y. X. W. acknowledge the Chinese Scholarship Council for supporting his visit to Florida State University (No. 201706460046). A portion of this work was supported by the COMSATS University, Islamabad.

References

1 R. Gilchrist, R. Medal, W. D. Shorey, R. C. Hanselman, J. C. Parrott and C. B. Taylor, Selective inductive heating of lymph nodes, *Ann. Surg.*, 1957, **146**(4), 596.
2 M. Johannsen, *et al.*, Morbidity and quality of life during thermotherapy using magnetic nanoparticles in locally recurrent prostate cancer: results of a prospective phase I trial, *Int. J. Hyperthermia*, 2007, **23**(3), 315–323.
3 J. Carrey, B. Mehdaoui and M. Respaud, Simple models for dynamic hysteresis loop calculations of magnetic single-domain nanoparticles: application to magnetic hyperthermia optimization, *J. Appl. Phys.*, 2011, **109**(8), 083921.
4 E. L. Verde, G. T. Landi, J. d. A. Gomes, M. H. Sousa and A. F. Bakuzis, Magnetic hyperthermia investigation of cobalt ferrite nanoparticles: comparison between experiment, linear response theory, and dynamic hysteresis simulations, *J. Appl. Phys.*, 2012, **111**(12), 123902.
5 Q. Pankhurst, N. Thanh, S. Jones and J. Dobson, Progress in applications of magnetic nanoparticles in biomedicine, *J. Phys. D: Appl. Phys. Ann. Surg.*, 2009, **42**(22), 224001.
6 M. S. Carrião, V. R. Aquino, G. T. Landi, E. L. Verde, M. H. Sousa and A. F. Bakuzis, Giant-spin nonlinear response theory of magnetic nanoparticle hyperthermia: a field dependence study, *J. Appl. Phys.*, 2017, **121**(17), 173901.

7 I. Baker, Q. Zeng, W. Li and C. R. Sullivan, Heat deposition in iron oxide and iron nanoparticles for localized hyperthermia, *J. Appl. Phys.*, 2006, **99**(8), 08H106.
8 L.-Y. Zhang, H.-C. Gu and X.-M. Wang, Magnetite ferrofluid with high specific absorption rate for application in hyperthermia, *J. Magn. Magn. Mater.*, 2007, **311**(1), 228–233.
9 A. ur Rashid, A. Humayun and S. Manzoor, $MgFe_2O_4/ZrO_2$ composite nanoparticles for hyperthermia applications, *J. Magn. Magn. Mater.*, 2017, **428**, 333–339.
10 R. Hergt, S. Dutz, R. Müller and M. Zeisberger, Magnetic particle hyperthermia: nanoparticle magnetism and materials development for cancer therapy, *J. Phys.: Condens. Matter*, 2006, **18**(38), S2919.
11 G. C. Papaefthymiou, Nanoparticle magnetism, *Nano Today*, 2009, **4**(5), 438–447, DOI: 10.1016/j.nantod.2009.08.006.
12 A. Jordan, R. Scholz, P. Wust, H. Fähling and R. Felix, Magnetic fluid hyperthermia (MFH): cancer treatment with AC magnetic field induced excitation of biocompatible superparamagnetic nanoparticles, *J. Magn. Magn. Mater.*, 1999, **201**(1), 413–419.
13 A. Jordan, *et al.*, Endocytosis of dextran and silan-coated magnetite nanoparticles and the effect of intracellular hyperthermia on human mammary carcinoma cells *in vitro*, *J. Magn. Magn. Mater.*, 1999, **194**(1), 185–196.
14 S. Dutz and R. Hergt, Magnetic nanoparticle heating and heat transfer on a microscale: basic principles, realities and physical limitations of hyperthermia for tumour therapy, *Int. J. Hyperthermia*, 2013, **29**(8), 790–800.
15 A. u. Rashid, A. Ahmed, S. N. Ahmad, S. A. Shaheen and S. Manzoor, Study of specific absorption rate of strontium doped lanthanum manganite nanoparticles for self-controlled hyperthermia applications, *J. Magn. Magn. Mater.*, 2013, **347**, 39–44, DOI: 10.1016/j.jmmm.2013.07.045.
16 D. Thapa, V. Palkar, M. Kurup and S. Malik, Properties of magnetite nanoparticles synthesized through a novel chemical route, *Mater. Lett.*, 2004, **58**(21), 2692–2694.
17 V. Nikiforov, *et al.*, Magnetism and Verwey transition in magnetite nanoparticles in thin polymer film, *J. Alloys Compd.*, 2013, **569**, 58–61.
18 S. Ahmad, Y. Akin and S. Shaheen, $Gd_5(Si, Ge)_4$ and Gd_2C compounds: candidates for hyperthermia treatment of cancer, *J. Appl. Phys.*, 2005, **97**(10), 10Q902.
19 A. A. El-Gendy, *et al.*, Ferromagnetic Gd_5Si_4 nanoparticles as T2 contrast agents for magnetic resonance imaging, *IEEE Magn. Lett.*, 2017, **8**, 1–4.
20 Z. Cheng, A. Al Zaki, J. Z. Hui, V. R. Muzykantov and A. Tsourkas, Multifunctional nanoparticles: cost *versus* benefit of adding targeting and imaging capabilities, *Science*, 2012, **338**(6109), 903–910.
21 S. G. Hunagund, S. M. Harstad, A. A. El-Gendy, S. Gupta, V. K. Pecharsky and R. L. Hadimani, Investigating phase transition temperatures of size separated gadolinium silicide magnetic nanoparticles, *AIP Adv.*, 2018, **8**(5), 056428.
22 V. Pecharsky, G. Samolyuk, V. Antropov, A. Pecharsky and K. Gschneidner, The effect of varying the crystal structure on the magnetism, electronic structure and thermodynamics in the $Gd_5(Si_xGe_{1-x})_4$ system near $x = 0.5$, *J. Solid State Chem.*, 2003, **171**(1), 57–68.
23 R. C. O'handley, *Modern magnetic materials: principles and applications*, Wiley, 2000.
24 M. Morales, C. Serna, F. Bødker and S. Mørup, Spin canting due to structural disorder in maghemite, *J. Phys.: Condens. Matter*, 1997, **9**(25), 5461.
25 S. Shukla, A. Banas and R. Ramanujan, Atomistic mechanism of cyclic phase transitions in Nd–Fe–B based intermetallics, *Intermetallics*, 2011, **19**(8), 1265–1273.
26 S. N. Ahmad, Y. Akin and S. A. Shaheen, $Gd_5(Si,Ge)_4$ and Gd_2C compounds: candidates for hyperthermia treatment of cancer, *J. Appl. Phys.*, 2005, **97**(10), 10Q902, DOI: 10.1063/1.1849052.
27 S. N. Ahmad and S. A. Shaheen, Optimization of $(Gd)_5Si_4$ based materials: a step toward self-controlled hyperthermia applications, *J. Appl. Phys.*, 2009, **106**(6), 064701, DOI: 10.1063/1.3190556.
28 E. P. Nóbrega, N. A. d. Oliveira, P. J. v. Ranke and A. Troper, The magnetocaloric effect in R_5Si_4 (R = Gd, Tb): a Monte Carlo calculation, *J. Phys.: Condens. Matter*, 2006, **18**(4), 1275–1283, DOI: 10.1088/0953-8984/18/4/013.
29 S. Vasseur, *et al.*, Lanthanum manganese perovskite nanoparticles as possible *in vivo* mediators for magnetic hyperthermia, *J. Magn. Magn. Mater.*, 2006, **302**(2), 315–320.
30 S. C. Wuang, K. G. Neoh, E.-T. Kang, D. W. Pack and D. E. Leckband, Synthesis and functionalization of polypyrrole-Fe_3O_4 nanoparticles for applications in biomedicine, *J. Mater. Chem.*, 2007, **17**(31), 3354–3362.
31 S. Larumbe, C. Gomez-Polo, J. Pérez-Landazábal and J. Pastor, Effect of a SiO_2 coating on the magnetic properties of Fe_3O_4 nanoparticles, *J. Phys.: Condens. Matter*, 2012, **24**(26), 266007.
32 L. Blaney, *Magnetite (Fe_3O_4): Properties, synthesis, and applications*, 2007.
33 S. C. Wuang, K. G. Neoh, E.-T. Kang, D. W. Pack and D. E. Leckband, Synthesis and functionalization of polypyrrole-Fe_3O_4 nanoparticles for applications in biomedicine, *J. Mater. Chem.*, 2007, **17**(31), 3354–3362.
34 S. Yakushkin, A. Dubrovskiy, D. Balaev, K. Shaykhutdinov, G. Bukhtiyarova and O. Martyanov, Magnetic properties of few nanometers ε-Fe_2O_3 nanoparticles supported on the silica, *J. Appl. Phys.*, 2012, **111**(4), 044312.
35 E. L. Verde, *et al.*, Field dependent transition to the non-linear regime in magnetic hyperthermia experiments: comparison between maghemite, copper, zinc, nickel and cobalt ferrite nanoparticles of similar sizes, *AIP Adv.*, 2012, **2**(3), 032120.
36 A. Franco Jr and F. e Silva, High temperature magnetic properties of cobalt ferrite nanoparticles, *Appl. Phys. Lett.*, 2010, **96**(17), 172505.
37 N. K. Thanh, *et al.*, Cation distribution in $CuFe_2O_4$ nanoparticles: effects of Ni doping on magnetic properties, *J. Appl. Phys.*, 2016, **120**(14), 142115.
38 S. Deka and P. Joy, Superparamagnetic nanocrystalline $ZnFe_2O_4$ with a very high Curie temperature, *J. Nanosci. Nanotechnol.*, 2008, **8**(8), 3955–3958.